Twin-CQCM and Twin-TQCM Sensors With Wide Operating Temperature Range for Outgassing and Atomic Oxygen Measurement

Yuta Tsuchiya, Hiroyuki Kukita, Tsuyoshi Shiobara, Kazuki Yukumatsu, and Eiji Miyazaki

***Abstract*—In this paper, we propose a new Quartz Crystal Microbalance (QCM) sensor with temperature control, which can assess outgassing properties during spacecraft development. It will be referred to as the "Twin-QCM sensor." There are two types. The Twin-Cryogenic QCM (Twin-CQCM) sensor is warmed by a built-in heater with an operating temperature of –190 to +125°C, and the Twin-Thermoelectric QCM (Twin-TQCM) sensor is warmed and cooled by a built-in Peltier module that can control the temperature within –80 to +125°C. Using a temperature compensation technique, the temperature-dependent drift of the frequency was found to be less than ±10 ppm over all operating temperatures. An RTD temperature sensor was mounted on the quartz crystal to improve the accuracy of temperature measurement. To confirm the accuracy, an additional temperature sensor installed at the center of the crystal. The sensor output temperature value was compared to that of the additional sensor, with the difference between both temperature sensors being +0.4 to +2.6°C in the temperature range from –130 to +100°C. Through the measurement of the sensor's dynamic range, it was found that the deposited contaminant film in a vacuum increasingly changed such physical properties as viscoelasticity as the temperature increases.**

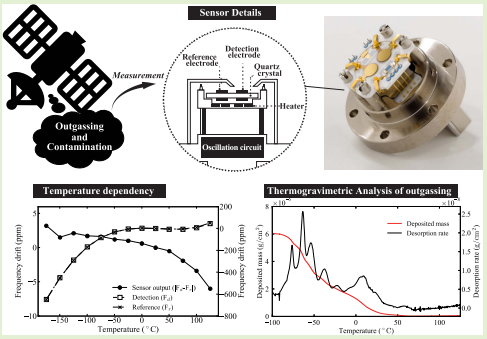

***Index Terms*—Quartz crystal microbalance (QCM), temperature compensation, spacecraft, outgas, contamination, atomic oxygen.**

I. Introduction

IN SPACECRAFT development, polymeric materials such as adhesives can generate contamination within a spacecraft. If outgassing from organic materials occurs under vacuum and produces deposits on spacecraft surfaces, the deposits can degrade the performance of onboard cameras, sensors, solar arrays, and thermal functional materials [1]–[8]. The temperature of a solar array typically exceeds 100°C in a vacuum because of incident solar radiation and, under these conditions, the adhesives used in the satellite can outgas easily. Whereas the temperature of a spacecraft surface facing away from the sun can fall below –20°C, outgassed deposits have a high probability of sticking. To prevent this contamination, materials for use in space are screened in accordance with established standards [9], [10] and simulation tools that emulate both outgassing and deposition kinetics to assess the amount of contaminant deposition in orbit [11], [12]. The QCM sensor is widely used to assess the deposition/desorption amounts of contaminants in a vacuum chamber, which simulates conditions in space such as extreme temperatures [3]. Because contamination depends strongly on temperature from –60 to +125°C, any sensor used for in-situ contamination measurement must have a wide operating temperature range. The operation of commercial QCM sensors is generally guaranteed only around room temperature, so their use cannot be extended to space use. Because the oscillation of a quartz crystal depends on its temperature, a technique for compensating for frequency drift is needed if only the mass effect of contamination phenomena is to be extracted. Some QCM sensors have been developed for space use [3], [13], [14]. They use two sensor crystals to compensate for the temperature effect. In particular, [15] summarizes the history of QCM sensors for space use. One sensor crystal is used to detect the deposited contaminant mass (ΔF_d), and the other is used to detect the frequency drift caused by the temperature effect on a reference frequency (ΔF_r). The sensor output frequency (F) is calculated from the two

Manuscript received December 26, 2020; accepted January 26, 2021. Date of publication February 10, 2021; date of current version April 5, 2021. The associate editor coordinating the review of this article and approving it for publication was Prof. Sheng-Shian Li. *(Corresponding author: Yuta Tsuchiya.)*

Yuta Tsuchiya, Tsuyoshi Shiobara, Kazuki Yukumatsu, and Eiji Miyazaki are with the Research and Development Directorate, Japan Aerospace Exploration Agency, Tsukuba 305-8505, Japan (e-mail: tsuchiya.yuta@jaxa.jp).

Hiroyuki Kukita is with Nihon Dempa Kogyo, Chitose 066-0009, Japan.

Digital Object Identifier 10.1109/JSEN.2021.3058324

frequencies ($|F_d - F_r|$). The deposited as mass on QCM sensor is converted by the Sauerbrey equation, Eq. (1), where ΔF ($= |\Delta F_d - \Delta F_r|$) and Δm are the frequency shift and deposited mass, respectively; f_0 is the resonant frequency, A is the electrode area, ρ_q is the density of quartz, and μ_q is the shear modulus of AT-cut quartz crystal. For the Twin-CQCM, A, f_0, ρ_q *and* μ_q are 12.6 mm^2, 10.278 MHz, 2.65 g/cm^3, and 2.95×10^{11} g/cm/s^2, respectively. The mass sensitivity of the QCM sensor is defined by Eq. (2).

$$\Delta F = -\frac{2f_0^2}{A\sqrt{\rho_q \mu_q}}\Delta m \tag{1}$$

$$\text{Mass sensitivity}: \frac{\Delta F}{\Delta m} = -\frac{2f_0^2}{A\sqrt{\rho_q \mu_q}} \tag{2}$$

However, the use of two separate quartz crystals complicates crystal replacement due to the sensor structure. Furthermore, because the sensor temperature is measured at a distance from the area whose temperature is to be sensed, the error between the sensing area and the sensor output has not been discussed yet. On the other hand, once contaminant substances irreversibly adhere to the sensor crystal, the sensor output frequency (F_d) gradually increases according to the remaining contaminants that cannot be removed by bake-out. Therefore, a technique for refreshing the sensor surface is needed to maintain the sensor in good condition for contamination tests.

This paper proposes a twin-electrode technique to simplify the sensor structure, to measure the crystal temperature directly, and to enable easy sensor replacement. The proposed structure also improves reconciling each electrode's temperature and its temperature dependence without need for a crystal matching test. The Twin-Cryogenic QCM (Twin-CQCM) sensor is cooled by liquid nitrogen and warmed by a built-in heater. The Twin-Thermoelectric QCM (Twin-TQCM) sensor is cooled and warmed by a Peltier unit inside the sensor. The Twin-TQCM sensor can be used without a coolant liquid in either a vacuum or in atmosphere. Moreover, this sensor can easily be used to measure Atomic Oxygen (AO) flux. Atomic oxygen is the most significant concern for Low Earth Orbit (LEO) satellites [16], [17]. When atomic oxygen, which is found mainly at altitudes under 300 km, collides with a satellite, it interacts strongly with the satellite materials because of its high physical energy.

Sections II and III of this paper describes the proposed twin-electrode design based on the Twin-CQCM sensor. The Twin-TQCM sensor is discussed in Section IV. Section V describes the ease of replacing the sensor crystal, which is essential to expand its applications, for example, as an atomic oxygen sensor, described in Section V.

II. Twin-Electrode Sensor Crystal

Figure 1 shows the twin-electrode sensor crystal including the two oscillation electrodes for detection (F_d) and reference (F_r). The reference electrode is placed next to the detection electrode to prevent interaction with the adjacent electrode. The oscillation electrodes and the quartz crystal are 4 mm and 14 mm in diameter, respectively. The crystal is 162 μm thick, and the oscillator operates in the fundamental mode

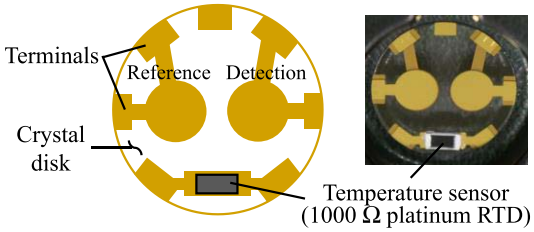

Fig. 1. The twin-electrode sensor crystal including the electrodes for detection and reference. At the left is the electrode pattern drawing, at the right is a photo of the crystal. The RTD sensor is placed close to the oscillation electrodes so as not to affect the oscillation energy field.

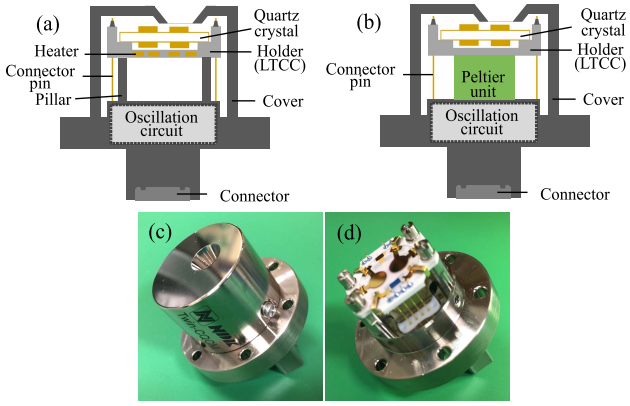

Fig. 2. Cross-section drawings of the (a) Twin-CQCM and (b) Twin-TQCM sensor units. (c) Photo of the Twin-CQCM sensor unit with the cover. (d) without the cover.

at 10.278 MHz. A resistance temperature detector (RTD) is installed on the same quartz crystal using the free area to measure the crystal temperature itself for improved accuracy. Given the sensitive reaction to temperature conditions by contamination phenomena, accurate temperature measurement is meaningful. A commercial RTD is used, whose characteristics are calibrated by the manufacturer. This is an advantage over an RTD surface electrode pattern unless the additional sensor does not interact with the oscillation mode.

There are six terminals along the edge of the quartz crystal for small clips to clamp the quartz crystal, and the Low Temperature Co-fired Ceramics (LTCC) holder (Fig. 2) without any mechanical strain. The heater for temperature control is embedded in the LTCC holder. The connector pins transmit the oscillation frequency signals, heater current, and temperature sensor signal. The Twin-CQCM sensor provides two kinds of signals: one for fundamental mode frequency (10.278 MHz), and the other for 3rd overtone mode frequency (30.834 MHz). Operating the sensor in its 3rd overtone mode multiplies the sensor sensitivity by three. Table I summarizes the basic sensor specifications. The detection and reference electrodes are 5 mm apart, center-to-center. To prevent the vibration interference between the electrodes, the electrodes' oscillation is excited alternately: (1) fundamental mode at the reference electrode, (2) 3rd overtone/reference, (3) 3rd overtone/detection, (4) fundamental/detection. Thus, the sensor provides four individual signals over one frequency signal line as a time division by changing the state of selectors built into the oscillation circuit shown in Fig. 2. The controller outside

TABLE I
TWIN-QCM SPECIFICATIONS

Item	Value
Oscillation frequency: f_0	10.278 MHz
Quartz crystal	AT-cut / 14 mm diameter Twin-electrodes
Electrode diameter	4 mm
Electrode area: A	12.6 mm^2
Mass sensitivity: $\frac{\Delta F}{\Delta m}$	2.39×10^8 (Fund.) Hz/(g/cm^2) 7.17×10^8 (3rd.) Hz/(g/cm^2)
Temperature sensor	RTD platinum 1000 Ω
Operating temperature	Twin-CQCM: −190 to +125°C Twin-TQCM: −80 to +125°C

the vacuum chamber provides the selector signals and receives the four frequency signals once every second.

As the quartz crystal is held in place on the LTCC holder using six small clips, the user can easily replace the quartz crystal in a few minutes without complicated instructions. Regarding the investigation of UV enhancement phenomena of contamination [18], the ease of replaceability is an excellent feature because contaminants tend to irreversibly adhere, especially under UV irradiation, and degrade sensor stability especially the F-T characteristics. Thanks to this advantage, the user can perform any contamination tests under UV irradiation with a sensor in good condition.

A. Outgas Deposition Simulation and Validation

The reference electrode has a sensor cover as Fig. 2 shows and should not be sensitive to outgas deposition. On the other hand, because a gap is needed between the quartz crystal and the cover for the crystal to oscillate, outgas deposits may form on the reference electrode through this gap, depending on the cover design, because of the multi-reflection effect of the gas, the contaminant might reach the reference crystal through the tiny gap. Therefore, some outgas deposition simulations were conducted to roughly estimate the amount of the outgas depositing onto the reference electrode. Japanese SPacecraft Induced Contamination Environment analysis software (J-SPICE) [19] is a simulation tool for predicting outgassing from materials and deposition on a surface at various temperatures in a vacuum. The outgas model is defined as follows:

$$\frac{dm}{dt} = \frac{dM(t)}{dt} \cdot F \cdot s\,(T_R) \tag{3}$$

$$M(t) = a \cdot t^b + c \tag{4}$$

$$s\,(T_R) = f \cdot (T_R - T_0) + 1 \tag{5}$$

where dm/dt is the deposition rate, $dM(t)/dt$ is the outgas rate from material samples changing in accordance with time (t), and F is the view factor between the contaminated surface and the contamination source material, which is calculated using Thermal Desktop^{TM}(C&R Technologies) functions. $M(t)$ in Eq. (4) is the outgas parameter that depends on each outgassing source material: a, b, and c are constants, and t is time. Here, a, b, and c were set to 2.4×10^{-7}, 0.37 and 0, respectively; these parameters were obtained through experiment using an epoxy adhesive EC2216 (3M Scotch-Weld^{TM}). $s(T_R)$ in Eq. (5) represents the sticking coefficient of outgas,

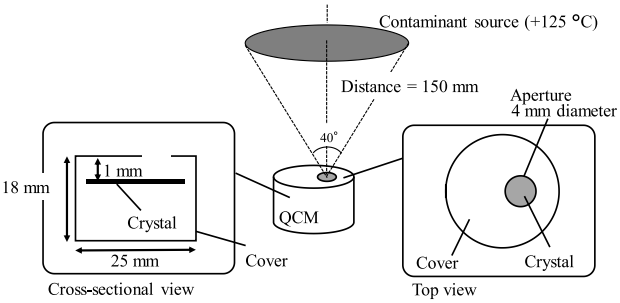

Fig. 3. Simulation geometry images. The distance between the contaminant source and the QCM is 150 mm. The crystal was placed 1 mm behind the sensor cover.

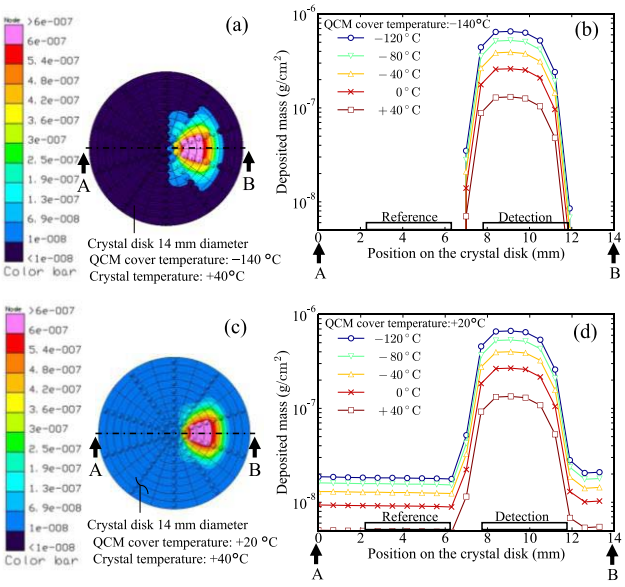

Fig. 4. Simulation results of deposited mass prediction at each temperature condition on the quartz crystal surface considering the sensor cover. (a) and (b) are results when the QCM cover temperature is −140°C. (c) and (d) are results when the QCM cover temperature is set to +20°C in the worst case.

where T_R is the temperature of the contaminated surface, and T_0 is the temperature of contaminated surface when the sticking coefficient reaches 1.0. f is a constant with a value of -5×10^{-4}. Equation (3) describes the sticking coefficient changes as a function of temperature. The molecular flux transportaion is calculated using the same method as does NASA's MOLFLUX (version 2.0) [20] Figure 3 shows images of the simulation geometry, where the conaminant source behavior follows Eq (4). Based on the geometry, the view factor was calclated. Figure 4 shows the calculated deposited mass after 10 days; (a) and (b) are of the deposited mass when the QCM case temperature is set to −140°C (when it was installed on a metallic base plate cooled by liquid nitrogen [i.e., the Twin-CQCM]). In each case, the deposited mass at the reference electrode is much less than at the detection one. Figures 4(c) and (d) are for the deposited mass when the QCM case temperature is +20°C, assuming the Twin-TQCM use in the worst case under one atmosphere, because heat applied to the sensor case enhances the multi-reflection effect. At each crystal temperature, from −120 to +40°C,

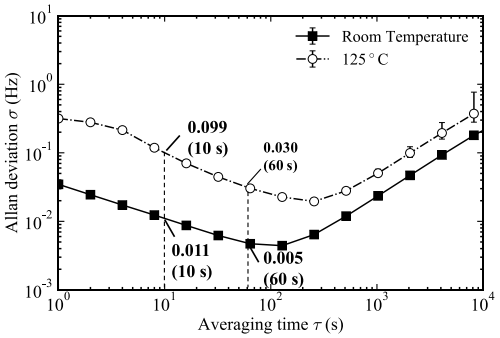

Fig. 5. Short-term stability (Allan deviation) experimental results of the Twin-CQCM sensor at room temperature without temperature control and +125 °C under a vacuum. When the averaging time was 10 seconds, the deviation was 0.011 Hz and 0.099 Hz at room temperature and +125 °C, respectively.

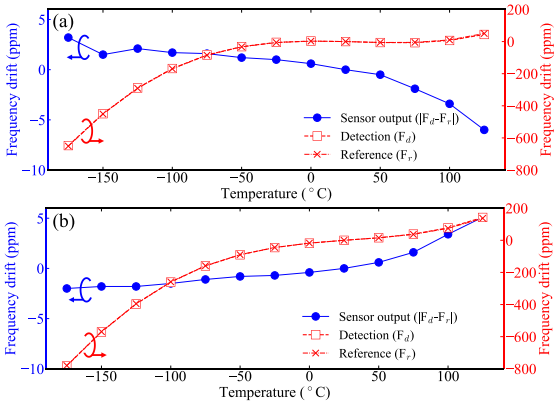

Fig. 6. Twin-CQCM frequency drift in (a) fundamental and (b) 3rd overtone mode caused by temperature dependency.

the deposition ratio for reference over detection was 0.026 to 0.036, thereby securing an acceptable ratio for contamination measurements based on the results.

B. Sensor Short Term Stability and Resolution

Figure 5 shows the short-term stability of the Twin-CQCM sensor in the fundamental mode for the values of Allan deviation with a one-second sampling period. When the averaging time was 10 seconds, the frequency deviations were 0.011 Hz and 0.099 Hz at room temperature and +125°C, respectively. When it was 60 seconds, the values were 0.005 Hz and 0.030 Hz; therefore, the output frequency is sufficiently stable for contamination measurement even at +125°C because 0.1 Hz (ΔF) represents 0.42 ng/cm^2, which is sufficient resolution for contamination measurement. According to this result, the directly bonded RTD sensor and the small clips do not affect the stability at either room temperature or +125°C.

C. Frequency-Temperature (F-T) Characteristics

The operating temperature of the Twin-CQCM sensor ranges from –190 to +125°C. Figure 6 shows the frequency drift caused by the temperature-dependent effect of quartz crystal in both modes. The drift of both detection and reference frequency was investigated, while the temperature of the Twin-CQCM was swept from –190 to +125°C by the built-in heater

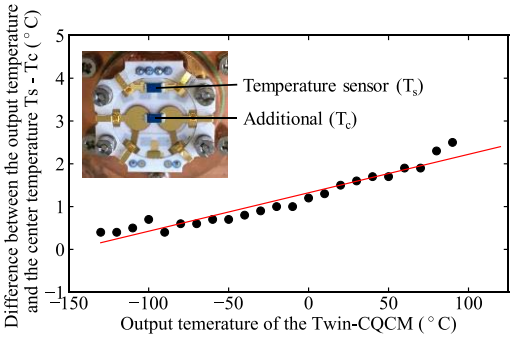

Fig. 7. Twin-CQCM temperature measurement accuracy when the Twin-CQCM was cooled to –190°C. The difference between the two RTDs was less than 2.6°C. The error was 0.4°C at –130°C.

in a vacuum chamber. The Twin-CQCM was attached to a copper baseplate cooled by liquid nitrogen. Thanks to the twin-electrode technique, the drift of the output frequency was less than ±10 ppm ($|F_d - F_r|$) in the range of –175 to +125°C without the crystal matching procedure in selecting a pair of crystals with the same temperature dependencies. The value for delta is sufficiently small that it does not affect estimation of the contaminant deposition/desorption mass.

D. Temperature Measurement Accuracy

As shown in Fig. 1, a temperature sensor is installed in the free area of the crystal to measure the crystal temperature directly. Because the temperature of interest is at the electrodes, (i.e., the center of the crystal), the difference between the sensor temperature (T_s) and the center temperature (T_c) was estimated. Figure 7 shows the result of the difference. To measure the center temperature, an additional sensor (T_c) was installed. The sensing and reference electrodes instead of the oscillation function. The difference between the two temperature sensors ($T_s - T_c$) was +0.4 to +2.6°C in the range of –130 to +100°C under cooling by liquid nitrogen. The slope was only 0.009, which confirmed the accuracy of temperature measurement. Because the baseplate was controlled at –190°C by liquid nitrogen, the error value was larger the further away the crystal temperature was from the baseplate temperature. For more accurate temperature measurement, it is better for the baseplate temperature should be kept as close to the temperature range of interest as possible.

III. Contamination Measurement

A. Deposition and Desorption Sensing

To verify the sensor functions, a contamination measurement was conducted using a vacuum chamber as shown in Fig. 8. The apparatus consists of an Effusion Cell including a contaminant source and a Twin-CQCM sensor facing the Effusion Cell. The Effusion Cell is a cylindrical metallic case with an orifice at the bottom and a heater around the side to warm the source material inside it. Figure 9 shows an outgas deposition and desorption measurement of an epoxy adhesive, EC2216. The deposition was clearly confirmed from the sensor frequency change ($\Delta F = |\Delta F_d - \Delta F_r|$) in the deposition phase at the sensor temperature of –20°C. The

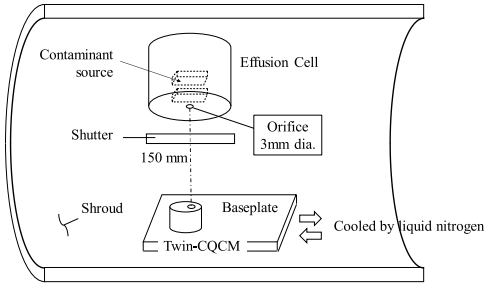

Fig. 8. Vacuum chamber setup for the contamination test to verify the Twin-CQCM sensor functions. Both the baseplate and the shroud were cooled by liquid nitrogen to prevent multi-reflection of outgas and to keep the sensor at –190°C.

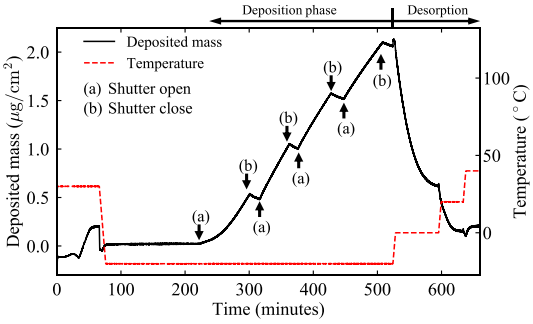

Fig. 9. Deposition and desorption experiment result of the Twin-CQCM sensor from −20 to +125°C. At each plateau in the deposition phase, the sensor was evacuated under the gas flow.

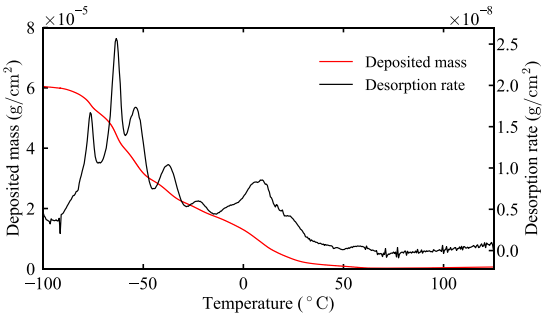

Fig. 10. TGA result of RTV-S691 from –100 to +125°C with a ramp rate of 1°C/min. Each peak represents a certain substance containing the adhesive.

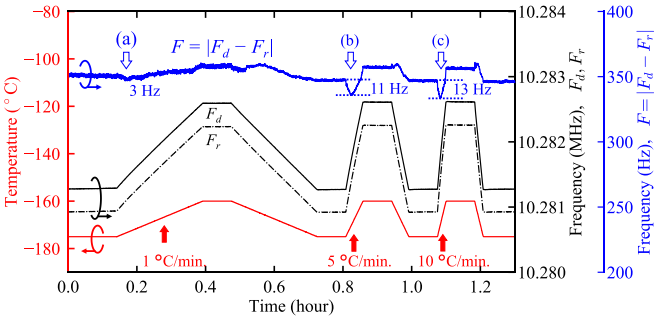

Fig. 11. Twin-CQCM frequency response to temperature change. The response was evaluated with three ramp rates at −175°C to −160°C in a vacuum chamber without deposition. The black solid and dash-dotted line represent detection (F_d) and reference frequency (F_r), respectively. The blue line shows sensor output frequency ($F = |F_d - F_r|$) The sensor output frequency disturbance with ramp rate of 1, 5, and 10°C per minute were 3, 11, and 13Hz, respectively.

deposition was interrupted by moving the shutter above the Twin-CQCM sensor with the baseplate from under the orifice at each plateau in Fig. 9. The reference frequency change (ΔF_r) was only –0.69 Hz from 200 s to 500 s (the data is not shown in Fig. 9); therefore, the sensor cover successfully kept the reference electrode clean. The result supports the calculated deposition distribution of the crystal as discussed in Section IIA. After the deposition phase, the sensor was warmed to 0, +20, +40 and +125°C to obtain the desorption characteristics. At a temperature between 0 and +20°C, the desorption characteristics of EC2216 were confirmed, which is consistent with our prior experimental results.

Thermogravimetric Analysis (TGA) [10], [14] is required to identify the number of different contaminants and to determine their desorption temperatures. The temperature of the sensors was set to –175°C at the deposition phase, and then the TGA spectrum was acquired at a ramp rate of 1°C per minute. The deposited mass acquired by the Twin-CQCM sensor was 60.0 μg/cm^2. As seen in the TGA spectrum in Fig. 10, some typical peaks were confirmed in the different temperature range in accordance with the substances of the RTV-S691.

B. Frequency Response to Temperature Change

Frequency shift caused by except for mass loading must be avoided. When the temperature setting is changed, the thermal input and output condition at the quartz crystal would be agitated because the temperature controller changes from isothermal to the ramp state. As a result, the Twin-CQCM frequency could be unstable at such a temperature state change point. Considering the use case of the Twin-CQCM, the temperature setting is expected to be changed from isothermal to temperature ramp state for Thermogravimetric Analysis. Figure 11 shows the evaluation results of the frequency response with three ramp rates at from −175°C to −160°C in a vacuum chamber. The disturbance was evaluated by the sensor output frequency at each change point from isothermal to ramp state ((a)(b)(c) in Fig. 11). The sensor output frequency ($F = |F_d - F_r|$) shift with ramp rates of 1, 5, and 10°C per minute were (a)3, (b)11, and (c)13Hz, respectively. It is thought that the higher ramp rate, the local thermal condition at the quartz crystal changes with higher ramp rates. Because both the detection (F_d) and reference frequency (F_r) changed in the same direction as shown in Fig. 11, the disturbances of the sensor output frequency were sufficiently minimized to measure contaminants in deposition and desorption, in particular, with a ramp rate of 1°C per minute, standardized in [10].

C. Isolation Between Detection and Reference Electrodes

The detection and reference electrodes oscillate alternately to eliminate the vibration interference between the electrodes. The mass load effect isolation between the electrodes is another concern, (i.e., the mass load at the detection electrode must be negligible with respect to the reference one). To evaluate the isolation, the detection and reference frequency changes during the deposition phase were investigated. Figure 12

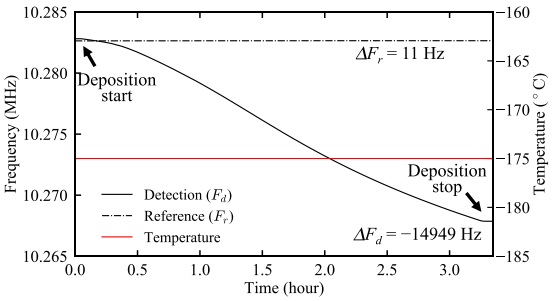

Fig. 12. Frequency behavior of both detection and reference electrodes during deposition phase. The source material was RTV-S691. The temperature of the Twin-CQCM was set to −175°C. The frequency change of the reference (ΔF_r) was only 11 Hz even though the detection (ΔF_d) was −14.949 kHz.

shows the frequency during deposition phase at −175°C, with source material of RTV-S691. The total frequency change of detection and reference was −14.949 kHz (ΔF_d) and 11 Hz (ΔF_r), respectively. It is found that the detection and reference electrode vibrations are well isolated, so the mass load at the detection electrode does not affect the reference one.

D. Sensor Dynamic Range

The dynamic range as a sensor frequency saturation was investigated with various source materials: RTV-S691, 2-ethylhexyl phthalate (DEHP), and polyimide film (U-varnish, UBE Industries) as shown in Table II. When the RTV-S691 was deposited, the fundamental mode frequency ($\Delta F = |\Delta F_d - -\Delta F_r|$) of 48.9 kHz (204.5 μg/cm^2) was confirmed in the deposition phase without no saturation as shown in Fig. 13(a). In the desorption phase after the deposition, the output frequency of 3rd overtone showed a unique response: the output frequency at the detection electrode jumped then stopped, even though it was less than the total deposited mass (204.5 μg/cm^2, at which pint it would become hard to oscillate). Because the oscillation drive margin of 3rd overtone is relatively less than that of the fundamental mode, the oscillation anomaly occurred only for the 3rd overtone. This suggests that properties such as density and viscosity of the deposited contaminant film on the QCM sensor changed according to the temperature increase. This behavior was noticeable with DEHP (Fig. 13(b)) even when the deposited mass was only 21.16 μg/cm^2 (5.057 kHz), much less than that of RTV-S691.

In contrast, saturation did not occur with polyimide film; the deposited mass was 705.9 μg/cm^2 (168.7 kHz). Because polyimide film (U-Varnish, UBE Industries) was coated using a spin coater on the detection electrode and cured at +350°C, the film was relatively stiff and less likely to absorb as much oscillation energy as RTV-S691 (silicone adhesive), and DEHP (liquid) did. Thus, the dynamic range varies and depends not only on the deposited mass but also the source material's physical properties.

The oscillation state in the desorption phase was investigated to identify the cause of the variation in saturation. The input-output throughput characteristics with the S parameter (S_{12}) of the fundamental mode was measured with RTV-S691

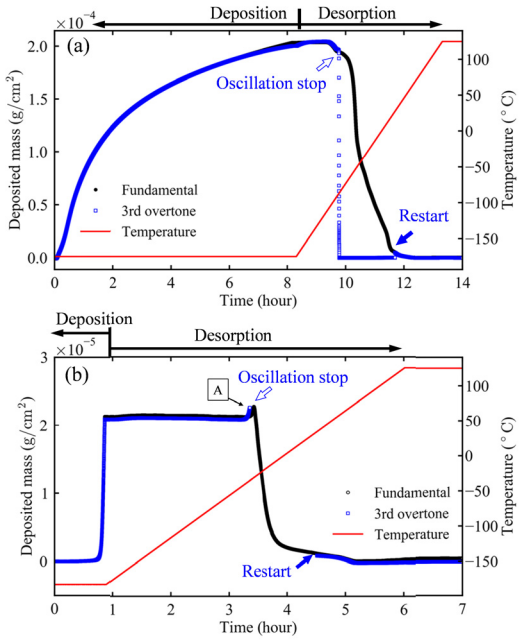

Fig. 13. The saturation characteristics of the Twin-CQCM. The black dots are the fundamental mode frequency (ΔF of fundamental), the blue dots are 3rd overtone frequency (ΔF of 3rd overtone). (a) The source material was RTV-S691, the total deposited mass was 204.5 μg/cm^2 (48.9 kHz). (b) DEHP, 21.16 μg/cm^2 (5.057 kHz).

source material. A network analyzer (Keysight E5100A) was connected to the detection electrode through a feedthrough into the vacuum chamber. Figure 14 shows S_{12} around the fundamental mode frequency (10.278 MHz) of the detection electrode obtained by the network analyzer during the desorption phase, where the resonance frequency was determined, and where the attenuation was at its minimum (i.e., maximum S_{12}). The S_{12} response showed two features: that the anomaly resonance frequency shifted from –90 to –70°C and that the oscillation impedance increased at –50°C. The resonance frequency decreased from –90 to –70°C (Figs. 14 (a)(b)(c)), although the deposited mass must have decreased (i.e., the resonance frequency must have increased). This is similar to the case of DEHP (Fig. 13(b)); the oscillation frequency decreased (i.e., as if the deposited mass increased) just before the oscillation stopped (A), even though it was in the desorption phase. Here, the relationship between oscillation frequency and liquid properties on the Twin-CQCM electrode is expressed in Eq. (6) [21].

$$\Delta F = -f_0^{\frac{3}{2}} \sqrt{\frac{\rho_l \mu_l}{\pi \rho_q \mu_q}} \tag{6}$$

Where, f_0, ρ_q, and μ_q are the parameters of quartz crystal, the same as with Eq. (1): ρ_l *and* μ_l are the density and viscosity of the liquid on the detection electrode. Based on Eq. (6), the Twin-CQCM frequency shifts when the density and viscosity of the liquid on the electrode change. Given that the deposited contaminant film effused from RTV-S691 and DEHP behaves like a viscoelastic medium, the frequency shift in Fig. 13(b) A and Figs. 14 (a)(b)(c) indicated an increase in the density (ρ_l) or the viscosity (μ_l). The oscillation impedance increase in

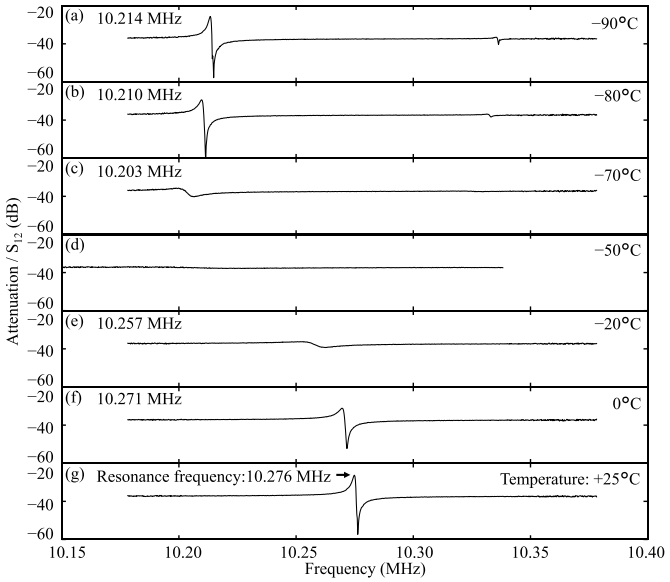

Fig. 14. Resonant response (S_{12}) of the Twin-CQCM sensor in desorption phase with silicone rubber. (a) was at temperature of –90°C at the end of deposition phase. Increasing the temperature, the S_{12} was changed from (a) to (g) at +25°C. The total deposited mass was 60.0 kHz (251.0 μg/cm^2).

TABLE II
TWIN-QCM SENSOR DYNAMIC RANGE

Source material	Saturated deposited mass (μg/cm^2)	Saturated sensor output frequency (kHz)
RTV-S691	Deposition at −190°C	
	> 204.6	> 48.9
	Desorption from −190 to +125°C	
	around 204.6	around 48.9
Phthalic acid (DEHP)	Deposition at −190°C	
	> 21.16	> 5.057
	Desorption from −190 to +125°C	
	around 21.16	around 5.057
Polyimide film	Deposition and desorption	
	> 705.9	> 168.7

Fig.14 (c)(d)(e) also suggests that the density and/or viscosity change caused the oscillation energy loss and the oscillation to stop. Based on these results, the sensor dynamic range strongly depends on the physical properties of the contaminant film, such as density and viscosity, as mentioned in [22].

Moreover, because the anomaly saturation occurred in the middle of desorption, the contaminant film properties, such as density and viscosity, drastically changed with warming in the desorption phase. Accordingly, these results prove that some kinds of contaminant films behave as viscoelastic media, and their properties change upon desorption under a vacuum. Thus, it is thus expected that the Twin-QCM, with its admittance measurement and analysis techniques [23], is suitable to the investigate property changes of contaminant films.

Table II summarizes the results during both the deposition and desorption cases. For RTV-S691 with a total deposited mass of 204.6 μg/cm^2, since the oscillation continued in the deposition, there was a margin for the oscillation to stop; conversely, since the 3rd overtone stopped in the desorption phase, the oscillation stop should occur around the deposited mass range (i.e., 204.6 μg/cm^2) also in the fundamental mode. Similarly, for DEHP, the dynamic range in the deposition and the desorption phase would be more than 21.16 μg/cm^2 and around 21.16 μg/cm^2, respectively. On the other hand, the dynamic range with polyimide film is well secured until 705.9 μg/cm^2 is reached in both the deposition and the desorption phases.

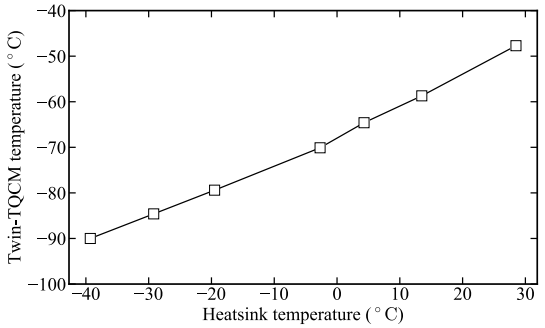

Fig. 15. The relationship of temperature between a copper heatsink and the Twin-TQCM temperature. The vertical axis shows the lowest Twin-TQCM temperature using the Peltier unit with maximum input power. The Twin-TQCM was installed on the heatsink cooled by a cooling bath to control the heatsink temperature.

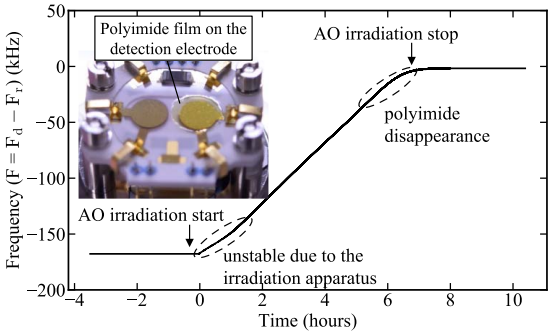

Fig. 16. AO fluence measurement by the Twin-CQCM sensor with polyimide thin film.

IV. TWIN-TQCM SENSOR

A new Twin-Thermoelectric QCM (TQCM) sensor was also developed. It does not require liquid nitrogen cooling. Instead of the heater in the LTCC holder, a two-stage Peltier unit is inserted between the holder and the oscillation circuit (Fig.2). The operating temperature with active control by the Peltier unit ranges from –80 to +125°C. The operating temperature with active control by the Peltier unit ranges from –80 to +125°C. The Peltier unit's cooling characteristics, represented by ΔT between the heatsink and the quartz crystal, apparently depends on the heatsink temperature and the surrounding thermal conditions. Figure 15 shows the relationship between the temperatures of a copper heatsink and a sensor crystal in vacuum. The heatsink was chilled by a cooling bath instead of by liquid nitrogen. When the heatsink was cooled below –30°C, the crystal temperature dropped below –80°C. When the heat sink was at +28.5°C (i.e., room temperature), the crystal temperature was –40°C. The Twin-TQCM sensor

assures that the ΔT between the heatsink and the sensor is at least 50°C if the thermal dissipation path is secured.

V. Atomic Oxygen Measurement

As with contamination phenomena, Atomic Oxygen (AO) 's degradation effects are investigated thoroughly and estimated in a vacuum. To demonstrate this application, an AO irradiation test was conducted using the vacuum chamber reported in earlier work [24]. A thin, polyimide film was selected as the target material for AO irradiation. The polyimide film is eroded in proportion to the number of AO collisions, and the Twin-CQCM sensor can measures the erosion rate. Figure 16 shows the sensor crystal with a polyimide film (U-Varnish, UBE Industries) coated using a spin coater on the sensor electrode for detection. When the thickness of the film was 5.4 μm, the frequency of the sensor was 168.7 kHz. The sensor was installed in an AO irradiation chamber, and another polyimide film sheet was put next to the Twin-CQCM sensor for monitoring the AO total fluence. Figure 16 shows the frequency during irradiation. The sensor successfully determined the AO flux and the number of AO particles incident per second (i.e., a slope of approximately 7 Hz/s), which is consistent with the sensitivity of 9.44 atoms/cm^2/Hz calculated for the reference polyimide film placed next to the Twin-CQCM sensor. The total AO flux during the irradiation test was calculated by Eq. (7).

$$F_{AO} = \frac{\Delta m}{A \rho R_e} \tag{7}$$

where, F_{AO} is the AO fluence, Δm is the mass loss of the polyimide film, A and ρ are the area and density of the film on the detection electrode, respectively, and R_e is the reaction efficiency of AO and polyimide (3.0×10^{-24} cm^3/AO atom) [25]. Because the polyimide film entirely covered the detection electrode, A was consistent with the electrode area (12.6 mm^2), and ρ was 1.4 g/cm^3. The start of AO irradiation in Fig. 16 was unstable; due to the irradiation apparatus. Note that the oscillation did not stop during the erosion phase even though the deposited mass of 705.9 μg/cm^2 (168.7 kHz) was much higher than RTV-S691 described in Section IIIB; this is because the polyimide film is not a viscoelastic medium.

VI. Conclusion

The new Twin-CQCM and Twin-TQCM with a wide operating temperature range for outgas assessment was proposed and demonstrated. The Twin-TQCM sensor is applicable for onboard spacecraft sensor because it needs no refrigerant for temperature control. This paper reports the sensors' excellent accuracy – the difference between the sensor output and the center of the crystal was less than 2.6°C. The Twin-QCMs had easy replaceability for sensor refreshment and can also be used to measure AO.

In the discussion on the dynamic range, it was stated that the saturation frequency varies with the type of deposited material. Twin-QCMs oscillated in contact with polyimide film at 168.7 kHz; in contrast, the oscillation quality was degraded in contact with DEHP even at 5.057 kHz in the desorption phase. The measured S_{12} characteristics suggest that the contaminant film's physical properties change significantly, like viscoelastic media in a vacuum. An additional measurement system for simultaneous resonance frequency, impedance, and admittance is needed to investigate further. If QCM sensors accurately determine viscosity and density, it would be useful to provide further information about the kinds of substances of contaminant films and to improve the contamination predicting methods.

Acknowledgment

The authors deeply thank Mr. T. Inoue (Advanced Engineering Services Co., Ltd.) for strong support in measurement and sample preparation.

References

[1] T. B. Stewart *et al.*, "Photochemical spacecraft self-contamination-laboratory results and systems impacts," *J. Spacecraft Rockets*, vol. 26, no. 5, pp. 358–367, 1989.

[2] V. E. Skurat, I. O. Leipunsky, I. O. Volkov, P. A. Pshechenkov, N. G. Beriozkina, and L. S. Gatsenko, "Changes of solar array surfaces on orbital station mir," *J. Spacecraft Rockets*, vol. 48, no. 1, pp. 53–58, Jan. 2011.

[3] B. Wood *et al.*, "MSX satellite flight measurements of contaminant deposition on a CQCM and on TQCMs," in *Proc. 35th Aerosp. Sci. Meeting Exhib.*, Jan. 1997, p. 841.

[4] D. A. Gregory, "Bidirectional reflectance distribution function measurement of molecular contaminants in the ultraviolet, vacuum ultraviolet, and visible ranges," *Opt. Eng.*, vol. 46, no. 11, Nov. 2007, Art. no. 113601.

[5] K. T. Luey, K. R. Olson, and D. J. Coleman, "Optical system contamination: Formation of films and droplets," *J. Astronomical Telescopes, Instrum., Syst.*, vol. 4, no. 3, Jun. 2018, Art. no. 036001.

[6] D. A. Gregory, "Mie scattering of growing molecular contaminants," *Opt. Eng.*, vol. 46, no. 3, Mar. 2007, Art. no. 033602.

[7] R. L. Harvey, "Spacecraft neutral self-contamination by molecular outgassing," *J. Spacecraft Rockets*, vol. 13, no. 5, pp. 301–305, 1976.

[8] R. W. Phillips, L. U. Tolentino, and S. Feuerstein, "Spacecraft contamination under simulated orbital environment," *J. Spacecraft Rockets*, vol. 14, no. 8, pp. 501–508, Aug. 1977.

[9] *Standard Test Method for Total Mass Loss and Collected Volatile Condensable Materials From Outgassing in a Vacuum Environment*, ASTM Standards E595-15, 2015.

[10] *Standard Test Method for Contamination Outgassing Characteristics of Spacecraft Materials*, ASTM Standards E1559-09, 2016.

[11] H. W. Babel, M. Hasegawa, C. Jones, and J. Fussell, "The effects of contamination from silicones and a modified-tefzel insulation on critical surfaces of the international space station," *Acta Astronautica*, vol. 40, nos. 2–8, pp. 95–104, Jan. 1997.

[12] J.-F. Roussel, T. Tondu, T. Paulmier, D. Faye, M. Van Eesbeek, and R. Rampini, "Progress on the physical approach to molecular contamination modeling," *J. Spacecraft Rockets*, vol. 48, no. 2, pp. 246–255, Mar. 2011.

[13] D. A. Wallance and S. A. Wallance, "Use of a cryogenically cooled QCM in conjunction with a programmable data acquisition system to detect and examine accreted mass on the sensing crystal caused by environmental contamination," *Proc. SPIE*, vol. 1165, pp. 424–431, Jan. 1990.

[14] M. Magni *et al.*, "Temperature sensitivity of a quartz crystal microbalance for TGA in space," in *Proc. 5th IEEE Int. Workshop Metrol. Aerosp. (MetroAeroSpace)*, Jun. 2018, pp. 629–633.

[15] F. Dirri, E. Palomba, A. Longobardo, E. Zampetti, B. Saggin, and D. Scaccabarozzi, "A review of quartz crystal microbalances for space applications," *Sens. Actuators A, Phys.*, vol. 287, pp. 48–75, Mar. 2019.

[16] B. R. Spady *et al.*, "Low-earth-orbit exposure of carbon-based materials aboard shuttle flight STS-46," *J. Spacecraft Rockets*, vol. 32, no. 6, pp. 1015–1017, Nov. 1995.

[17] B. A. Banks, A. Snyder, S. K. Miller, K. K. de Groh, and R. Demko, "Atomic-oxygen undercutting of protected polymers in low Earth orbit," *J. Spacecraft Rockets*, vol. 41, no. 3, pp. 335–339, May 2004.

[18] A. Pereira, J.-F. Roussel, M. Van Eesbeek, O. Schmeitzky, and D. Faye, "Experiments and physical modeling of ultraviolet-enhanced contamination from pure contaminants," *J. Spacecraft Rockets*, vol. 43, no. 2, pp. 402–409, Mar. 2006.
[19] S. Baba *et al.*, "Experimental measurement of the reflection behavior of contaminant molecules," *Proc. SPIE*, vol. 9196, Sep. 2014, Art. no. 919605.
[20] E. R. Rios, C. L. Lake, and R. T. Rodriguez, "MOLFLUX—Molecular flux user's manual revision 2.0," Lockheed Eng. Sci. Company, Tech. Rep., 1992.
[21] K. K. Kanazawa and J. G. Gordon, "The oscillation frequency of a quartz resonator in contact with liquid," *Anal. Chim. Acta*, vol. 175, pp. 99–105, 1985. [Online]. Available: https://www.sciencedirect.com/science/article/abs/pii/S000326700082721X?via%3Dihub
[22] I. D. Avramov, "A 0-phase circuit for QCM-based measurements in highly viscous liquid environments," *IEEE Sensors J.*, vol. 5, no. 3, pp. 425–432, Jun. 2005.
[23] Y. Seida, "Demonstration of QCM measurement of viscoelastic phase behavior of PVA sol in its freezing-thawing process," *Macromol. Symposia*, vol. 358, no. 1, pp. 176–181, Dec. 2015.
[24] H. Shimamura and E. Miyazaki, "Investigations into synergistic effects of atomic oxygen and vacuum ultraviolet," *J. Spacecraft Rockets*, vol. 46, no. 2, pp. 241–247, Mar. 2009.
[25] *Standard Practices for Ground Laboratory Atomic Oxygen Interaction Evaluation of Materials for Space Applications*, ASTM Standards E2089-00, 2006.

Yuta Tsuchiya was born in Tokyo, Japan, in 1987. He received the bachelor's and master's degrees in engineering from Waseda University, Tokyo, Japan, in 2009 and 2011, respectively.

In 2011, he joined Japan Aerospace Exploration Agency, Japan. His research interests are in the field of gas sensors, atomic oxygen sensors, outgassing models, RF MEMS devices, and integrated circuits such as CPUs and FPGAs with radiation tolerance technique. He developed onboard equipment to demonstrate a space grade FPGA, and now currently develops a CPU for space use.

Hiroyuki Kukita was born in Hokkaido, Japan in 1971. He received the bachelor's degree in engineering from the Chiba Institute of Technology in 1994.

From 1994 to 2005, he was an Engineer of Hitachi Kokusai Electric Inc. Since 2005, he has been an Engineer of NIHON DEMPA KOGYO CO., LTD. His research interests include mobile wireless systems and systems using quartz sensors.

Tsuyoshi Shiobara was born in Hokkaido, Japan, in 1959. He received the bachelor's degree in engineering from the Hokkaido Institute of Technology in 1982. From 1982 to 1997, he was an Engineer of Hitachi Video and Information System, Inc. In 1997, he joined Hitachi Kokusai Electric Inc., and in 2004, joined NIHON DEMPA KOGYO CO., LTD. Since 2020, he has been a member of Japan Aerospace Exploration Agency. His research interests include system design and hardware fields such as communication systems, biosensors and gas sensors.

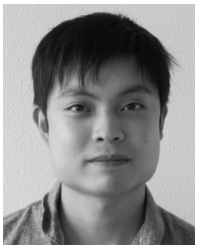

Kazuki Yukumatsu was born in Nara, Japan, in 1992. He received the bachelor's and master's degrees in engineering from Osaka University, Japan, in 2015 and 2017, respectively.

Since 2017, he has been a member of Japan Aerospace Exploration Agency, Japan. His research interest includes interaction between space environment and space materials, especially effect on polymeric materials by atomic oxygen and ultraviolet rays.

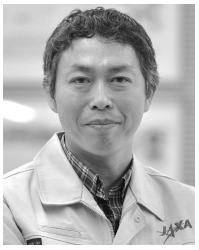

Eiji Miyazaki was born in Chitose, Hokkaido, Japan, in 1974, He received the bachelor's and master's degrees in materials science and engineering from Waseda University in 2008 and the Ph.D. degree in materials science and engineering from the Tokyo Institute of Technology in 2004.

From 1998 to 2000, he was an Engineer with Nagoya office of National Space Development Agency of Japan. From 2000 to 2003, he was a Research Associate with interdisciplinary Graduate School of Science and Engineering, Tokyo Institute of Technology. Since 2003, he has been an Associate Senior Researcher with the Research Unit I, Research and Development Directorate, Japan Aerospace Exploration Agency. His main research field is materials science and engineering for spacecraft such as: contamination on optical components for spacecraft caused by outgas emitted from other materials onboard; and interaction between space environment and materials on spacecraft, especially attack of atomic oxygen on materials in low earth orbit.